

---

# Score-based Generative Neural Networks for Large-Scale Optimal Transport

---

**Max Daniels**                      **Tyler Maunu \***                      **Paul Hand**  
Northeastern University      Brandeis University              Northeastern University  
daniels.g@northeastern.edu    maunu@brandeis.edu              p.hand@northeastern.edu

## Abstract

We consider the fundamental problem of sampling the optimal transport coupling between given source and target distributions. In certain cases, the optimal transport plan takes the form of a one-to-one mapping from the source support to the target support, but learning or even approximating such a map is computationally challenging for large and high-dimensional datasets due to the high cost of linear programming routines and an intrinsic curse of dimensionality. We study instead the Sinkhorn problem, a regularized form of optimal transport whose solutions are couplings between the source and the target distribution. We introduce a novel framework for learning the Sinkhorn coupling between two distributions in the form of a score-based generative model. Conditioned on source data, our procedure iterates Langevin Dynamics to sample target data according to the regularized optimal coupling. Key to this approach is a neural network parametrization of the Sinkhorn problem, and we prove convergence of gradient descent with respect to network parameters in this formulation. We demonstrate its empirical success on a variety of large scale optimal transport tasks.

## 1 Introduction

It is often useful to compare two data distributions by computing a distance between them in some appropriate metric. For instance, statistical distances can be used to fit the parameters of a distribution to match some given data. Comparison of statistical distances can also enable distribution testing, quantification of distribution shifts, and provide methods to correct for distribution shift through domain adaptation [12].

Optimal transport theory provides a rich set of tools for comparing distributions in *Wasserstein Distance*. Intuitively, an optimal transport plan from a source distribution  $\sigma \in \mathcal{M}_+(\mathcal{X})$  to a target distribution  $\tau \in \mathcal{M}_+(\mathcal{Y})$  is a blueprint for transporting the mass of  $\sigma$  to match that of  $\tau$  as cheaply as possible with respect to some ground cost. Here,  $\mathcal{X}$  and  $\mathcal{Y}$  are compact metric spaces and  $\mathcal{M}_+(\mathcal{X})$  denotes the set of positive Radon measures over  $\mathcal{X}$ , and it is assumed that  $\sigma, \tau$  are supported over all of  $\mathcal{X}, \mathcal{Y}$  respectively. The Wasserstein Distance between two distributions is defined to be the cost of an optimal transport plan.

Because the ground cost can incorporate underlying geometry of the data space, optimal transport plans often provide a meaningful correspondence between points in  $\mathcal{X}$  and  $\mathcal{Y}$ . A famous example is given by Brenier’s Theorem, which states that, when  $\mathcal{X}, \mathcal{Y} \subseteq \mathbb{R}^d$  and  $\sigma, \tau$  have finite variance, the optimal transport plan under a squared- $l_2$  ground cost is realized by a map  $T : \mathcal{X} \rightarrow \mathcal{Y}$  [26, Theorem 2.12]. However, it is often computationally challenging to exactly compute optimal transport plans, as one must exactly solve a linear program requiring time which is super-quadratic in the size of input datasets [5].

---

\*Work done while an Instructor in Applied Mathematics at MIT.

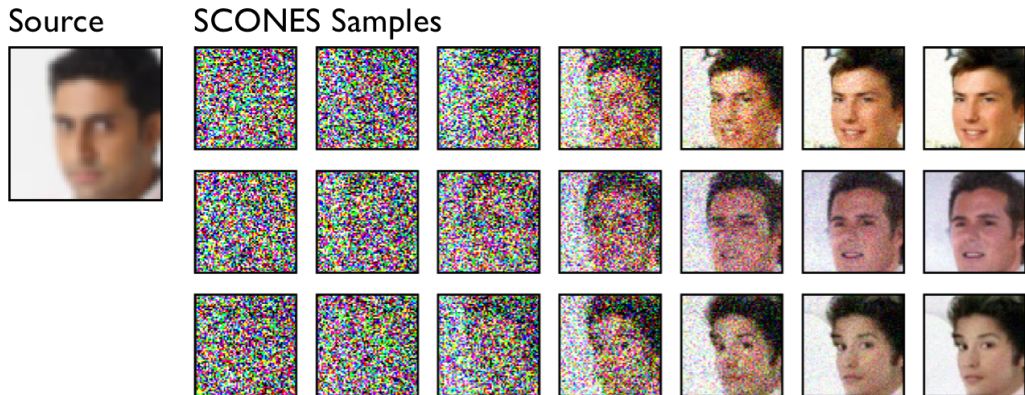


Figure 1: We use SCONES to sample the mean-squared- $L^2$  cost, entropy regularized optimal transport mapping between 2x downsampled CelebA images (Source) and unmodified CelebA images (Target) at  $\lambda = 0.005$  regularization.

Instead, we opt to study a regularized form of the optimal transport problem whose solution takes the form of a joint density  $\pi(x, y)$  with marginals  $\pi_X(x) = \sigma(x)$  and  $\pi_Y(y) = \tau(y)$ . A correspondence between points is given by the conditional distribution  $\pi_{Y|X=x}(y)$ , which relates each input point to a distribution over output points.

In recent work [22], the authors propose a large-scale stochastic dual approach in which  $\pi(x, y)$  is parametrized by two continuous dual variables that may be represented by neural networks and trained at large-scale via stochastic gradient ascent. Then, with access to  $\pi(x, y)$ , they approximate an optimal transport *map* using a barycentric projection of the form  $T : x \mapsto \arg \min_y \mathbb{E}_{\pi_{Y|X=x}}[d(y, Y)]$ , where  $d : \mathcal{Y} \times \mathcal{Y} \rightarrow \mathbb{R}$  is a convex cost on  $\mathcal{Y}$ . Their method is extended by [15] to the problem of learning regularized Wasserstein barycenters. In both cases, the Barycentric projection is observed to induce averaging artifacts such as those shown in Figure 2.

Instead, we propose a direct sampling strategy to generate samples from  $\pi_{Y|X=x}(y)$  using a *score-based generative model*. Score-based generative models are trained to sample a generic probability density by iterating a stochastic dynamical system known as *Langevin dynamics* [24]. In contrast to projection methods for large-scale optimal transport, we demonstrate that pre-trained score based generative models can be naturally applied to the problem of large-scale regularized optimal transport. Our main contributions are as follows:

1. We show that pretrained score based generative models can be easily adapted for the purpose of sampling high dimensional regularized optimal transport plans. Our method eliminates the need to estimate a barycentric projection and it results in sharper samples because it eliminates averaging artifacts incurred by such a projection.
2. Score based generative models have been used for unconditional data generation and for conditional data generation in settings such as inpainting. We demonstrate how to adapt pretrained score based generative models for the more challenging conditional sampling problem of *regularized optimal transport*.
3. Our method relies on a neural network parametrization of the dual regularized optimal transport problem. Under assumptions of large network width, we prove that gradient descent w.r.t. neural network parameters converges to a global maximizer of the dual problem. We also prove optimization error bounds based on a stability analysis of the dual problem.
4. We demonstrate the empirical success of our method on a synthetic optimal transport task and on optimal transport of high dimensional image data.

## 2 Background and Related Work

We will briefly review some key facts about optimal transport and generative modeling. For a more expansive background on optimal transport, we recommend the references [26] and [25].

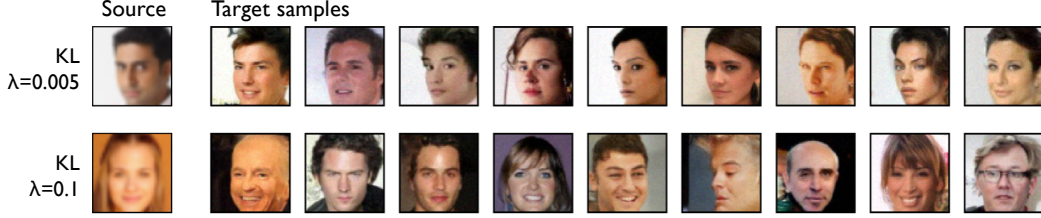


Figure 2: Samples generated by SCONES for entropy regularized optimal transport including the samples shown in Figure 1. At regularization  $\lambda = 0.005$ , optimal transportation with  $L^2$  cost has a visible effect on generated images. This effect diminishes at increased regularization  $\lambda = 0.1$ .

## 2.1 Regularized Optimal Transport

We begin by reviewing the formulation of the regularized OT problem.

**Definition 2.1** (Regularized OT). Let  $\sigma \in \mathcal{M}_+(\mathcal{X})$  and  $\tau \in \mathcal{M}_+(\mathcal{Y})$  be probability measures supported on compact sets  $\mathcal{X}, \mathcal{Y}$ . Let  $c : \mathcal{X} \times \mathcal{Y} \rightarrow \mathbb{R}$  be a convex, lower semi-continuous function representing cost of transporting a point  $x \in \mathcal{X}$  to  $y \in \mathcal{Y}$ . The regularized optimal transport distance  $\text{OT}_\lambda(\sigma, \tau)$  is given by

$$\begin{aligned} \text{OT}_\lambda(\sigma, \tau) &= \min_{\pi} \mathbb{E}_{\pi}[c(x, y)] + \lambda H(\pi) \\ \text{subject to } &\pi_X = \sigma, \quad \pi_Y = \tau \\ &\pi(x, y) \geq 0 \end{aligned} \quad (1)$$

where  $H : \mathcal{M}_+(\mathcal{X} \times \mathcal{Y}) \rightarrow \mathbb{R}$  is a convex regularizer and  $\lambda \geq 0$  is a regularization parameter.

We are mainly concerned with optimal transport of empirical distributions, where  $\mathcal{X}$  and  $\mathcal{Y}$  are finite and  $\sigma, \tau$  are empirical probability vectors. In most of the following theorems, we will work in the *empirical setting* of Definition 2.1, so that  $\mathcal{X}$  and  $\mathcal{Y}$  are finite subsets of  $\mathbb{R}^d$  and  $\sigma, \tau$  are vectors in the probability simplices of dimension  $|\mathcal{X}|$  and  $|\mathcal{Y}|$ , respectively.

We refer to the objective  $K_\lambda(\pi) = \mathbb{E}_{\pi}[c(x, y)] + \lambda H(\pi)$  as the *primal objective*, and we will use  $J_\lambda(\varphi, \psi)$  to refer to the associated *dual objective*, with dual variables  $\varphi, \psi$ . Two common regularizers are  $H(\pi) = \text{KL}(\pi || \sigma \times \tau)$  and  $H(\pi) = \chi^2(\pi || \sigma \times \tau)$ , sometimes called *entropy* and  $l_2$  regularization respectively:

$$\text{KL}(\pi || \sigma \times \tau) = \mathbb{E}_{\pi} \left[ \log \left( \frac{d\pi(x, y)}{d\sigma(x)d\tau(y)} \right) \right], \quad \chi^2(\pi || \sigma \times \tau) = \mathbb{E}_{\sigma \times \tau} \left[ \left( \frac{d\pi(x, y)}{d\sigma(x)d\tau(y)} \right)^2 \right]$$

where  $\frac{d\pi(x, y)}{d\sigma(x)d\tau(y)}$  is the Radon-Nikodym derivative of  $\pi$  with respect to the product measure  $\sigma \times \tau$ . These regularizers contribute useful optimization properties to the primal and dual problems.

For example,  $\text{KL}(\pi || \sigma \times \tau)$  is exactly the mutual information  $I_\pi(X; Y)$  of the coupling  $(X, Y) \sim \pi$ , so intuitively speaking, entropy regularization explicitly prevents  $\pi_{Y|X=x}$  from concentrating on a point by stipulating that the conditional measure retain some bits of uncertainty after conditioning. The effects of this regularization are described by Propositions 2.2 and 2.3.

First, regularization induces convexity properties which are useful from an optimization perspective.

**Proposition 2.2.** *In the empirical setting of Definition 2.1, the entropy regularized primal problem  $K_\lambda(\pi)$  is  $\lambda$ -strongly convex in  $l_1$  norm. The dual problem  $J_\lambda(\varphi, \psi)$  is concave, unconstrained, and  $\frac{1}{\lambda}$ -strongly smooth in  $l_\infty$  norm. Additionally, these objectives witness strong duality:  $\inf_{\pi \in \mathcal{M}_+(\mathcal{X} \times \mathcal{Y})} K_\lambda(\pi) = \sup_{\varphi, \psi \in \mathbb{R}^{2d}} J_\lambda(\varphi, \psi)$ , and the extrema of each objective are attained over their respective domains.*

In addition to these optimization properties, regularizing the OT problem induces a specific form of the dual objective and resulting optimal solutions.

**Proposition 2.3.** *In the setting of Proposition 2.2, the KL-regularized dual objective takes the form*

$$J_\lambda(\varphi, \psi) := \mathbb{E}_\sigma[\varphi(x)] + \mathbb{E}_\tau[\psi(y)] - \lambda \mathbb{E}_{\sigma \times \tau} \left[ \frac{1}{e} \exp \left( \frac{1}{\lambda} (\varphi(x) + \psi(y) - c(x, y)) \right) \right].$$

The optimal solutions  $\varphi^*, \psi^* = \arg \max_{\varphi, \psi \in \mathbb{R}^{2d}} J_\lambda(\varphi, \psi)$  and  $\pi^* = \arg \min_{\pi \in \mathcal{M}_+(\mathcal{X} \times \mathcal{Y})} K_\lambda(\pi)$  satisfy

$$\pi^*(x, y) = \frac{1}{e} \exp \left( \frac{1}{\lambda} (\varphi^*(x) + \psi^*(y) - c(x, y)) \right) \sigma(x) \tau(y).$$

These propositions are specializations of Proposition 2.4 and they are well-known to the literature on entropy regularized optimal transport [5, 2]. The solution  $\pi^*(x, y)$  of the entropy regularized problem is often called the *Sinkhorn coupling* between  $\sigma$  and  $\tau$  in reference to Sinkhorn's Algorithm [23], a popular approach to efficiently solving the discrete entropy regularized OT problem. For arbitrary choices of regularization, we call  $\pi^*(x, y)$  a Sinkhorn coupling.

Propositions 2.2 and 2.3 illustrate the main desiderata when choosing the regularizer: that  $H(\pi)$ , and hence  $K_\lambda(\pi)$ , be strongly convex in  $l_1$  norm and that  $H(\pi)$  induce a nice analytic form of  $\pi^*$  in terms of  $\varphi^*, \psi^*$ . In regards to the former,  $H(\pi)$  is akin to barrier functions used by interior point methods [5]. Prior work [2] is an example of the latter, in which it is shown that for discrete optimal transport,  $\chi^2$  regularization yields an analytic form of  $\pi^*$  having a thresholding operation that promotes sparsity.

Conveniently, the KL and  $\chi^2$  regularizers both belong to the class of  $f$ -Divergences, which are statistical divergences of the form

$$D_f(p||q) = \mathbb{E}_q \left[ f \left( \frac{p(x)}{q(x)} \right) \right].$$

where  $f : \mathbb{R} \rightarrow \mathbb{R}$  is convex,  $f(1) = 0$ ,  $p, q$  are probability measures, and  $p$  is absolutely continuous with respect to  $q$ . For example, the KL regularizer has  $f_{\text{KL}}(t) = t \log(t)$  and the  $\chi^2$  regularizer has  $f_{\chi^2}(t) = t^2 - 1$ . The  $f$ -Divergences are good choices for regularizing optimal transport: strong convexity of  $f$  is a sufficient condition for strong convexity of  $H_f(\pi) := D_f(\pi||\sigma \times \tau)$  in  $l_1$  norm, and the form of  $f$  is the aspect which determines the form of  $\pi^*$  in terms of  $\varphi^*, \psi^*$ . This relationship is captured by the following generalization of Propositions 2.2 and 2.3, which we prove in Section B of the Supplemental Materials.

**Proposition 2.4.** *Consider the empirical setting of Definition 2.1. Let  $f(v) : \mathbb{R} \rightarrow \mathbb{R}$  be a differentiable  $\alpha$ -strongly convex function with convex conjugate  $f^*(v)$ . Set  $f^{*'}(v) = \partial_v f^*(v)$ . Define the violation function  $V(x, y; \varphi, \psi) = \varphi(x) + \psi(y) - c(x, y)$ . Then,*

1. *The  $D_f$  regularized primal problem  $K_\lambda(\pi)$  is  $\lambda\alpha$ -strongly convex in  $l_1$  norm. With respect to dual variables  $\varphi \in \mathbb{R}^{|\mathcal{X}|}$  and  $\psi \in \mathbb{R}^{|\mathcal{Y}|}$ , the dual problem  $J_\lambda(\varphi, \psi)$  is concave, unconstrained, and  $\frac{1}{\lambda\alpha}$ -strongly smooth in  $l_\infty$  norm. Strong duality holds:  $K_\lambda(\pi) \geq J_\lambda(\varphi, \psi)$  for all  $\pi, \varphi, \psi$ , with equality for some triple  $\pi^*, \varphi^*, \psi^*$ .*
2.  *$J_\lambda(\varphi, \psi)$  takes the form  $J_\lambda(\varphi, \psi) = \mathbb{E}_\sigma[\varphi(x)] + \mathbb{E}_\tau[\psi(y)] - \mathbb{E}_{\sigma \times \tau}[H_f^*(V(x, y; \varphi, \psi))]$ , where  $H_f^*(v) = \lambda f^*(\lambda^{-1}v)$ .*
3. *The optimal solutions  $(\pi^*, \varphi^*, \psi^*)$  satisfy*

$$\pi^*(x, y) = M_f(V(x, y; \varphi, \psi)) \sigma(x) \tau(y)$$

$$\text{where } M_f(x, y) = f^{*'}(\lambda^{-1}v).$$

For this reason, we focus in this work on  $f$ -Divergence-based regularizers. Where it is clear, we will drop subscripts on regularizer  $H(\pi)$  and the so-called *compatibility function*  $M(v)$  and we will omit the dual variable arguments of  $V(x, y)$ . The specific form of these terms for KL regularization,  $\chi^2$  regularization, and a variety of other regularizers may be found in Section A of the Appendix.

## 2.2 Langevin Sampling and Score Based Generative Modeling

Given access to optimal dual variables  $\varphi^*(x)$ ,  $\psi^*(y)$ , it is easy to evaluate the density of the corresponding optimal coupling according to Proposition 2.4. To generate samples distributed according to this coupling, we apply *Langevin Sampling*. The key quantity used in Langevin sampling of a generic (possibly unnormalized) probability measure  $p(x)$  is its *score function*, given by  $\nabla_x \log p(x)$  for  $x \in \mathcal{X}$ . The algorithm is an iterative Monte Carlo method which generates approximate samples  $\tilde{x}_t$  by iterating the map

$$\tilde{x}_t = \tilde{x}_{t-1} + \epsilon \nabla_x \log p(\tilde{x}_{t-1}) + \sqrt{2\epsilon} z_t$$

where  $\epsilon > 0$  is a step size parameter and where  $z_t \sim \mathcal{N}(0, I)$  independently at each time step  $t \geq 0$ . In the limit  $\epsilon \rightarrow 0$  and  $T \rightarrow \infty$ , the samples  $\tilde{x}_T$  converge weakly in distribution to  $p(x)$ . Song and Ermon [24] introduce a method to estimate the score with a neural network  $s_\theta(x)$ , trained on samples from  $p(x)$ , so that it approximates  $s_\theta(x) \approx \nabla_x \log p(x)$  for a given  $x \in \mathcal{X}$ . To generate samples, one may iterate Langevin dynamics with the score estimate in place of the true score.

To scale this method to high dimensional image datasets, Song and Ermon [24] propose an annealing scheme which samples noised versions of  $p(x)$  as the noise is gradually reduced. One first samples a noised distribution  $p(x) * \mathcal{N}(0, \tau_1)$ , at noise level  $\tau_1$ . The noisy samples, which are presumed to lie near high density regions of  $p(x)$ , are used to initialize additional rounds of Langevin dynamics at diminishing noise levels  $\tau_2 > \dots > \tau_N > 0$ . At the final round, Annealed Langevin Sampling outputs approximate samples according to the noiseless distribution. Song and Ermon [24] demonstrate that Annealed Langevin Sampling (ALS) with score estimation can be used to generate sample images that rival the quality of popular generative modeling tools like GANs or VAEs.

## 3 Conditional Sampling of Regularized Optimal Transport Plans

Our approach can be split into two main steps. First, we approximate the density of the optimal Sinkhorn coupling  $\pi^*(x, y)$  which minimizes  $K_\lambda(\pi)$  over the data. To do so, we apply the large-scale stochastic dual approach introduced by Seguy et al. [22], which involves instantiating neural networks  $\varphi_\theta : \mathcal{X} \rightarrow \mathbb{R}$  and  $\psi_\theta : \mathcal{Y} \rightarrow \mathbb{R}$  that serve as parametrized dual variables. We then maximize  $J_\lambda(\varphi_\theta, \psi_\theta)$  with respect to  $\theta$  via gradient descent and take the resulting parameters  $\theta^*$  and the associated transport plan  $\hat{\pi}(x, y) = M(V(x, y; \varphi_{\theta^*}, \psi_{\theta^*}))\sigma(x)\tau(y)$ . This procedure is shown in Algorithm 1. Note that when the dual problem is only approximately maximized,  $\hat{\pi}$  need not be a normalized density. We therefore call  $\hat{\pi}$  the *pseudo-coupling* which approximates the true Sinkhorn coupling  $\hat{\pi}$ .

After optimizing  $\theta^*$ , we sample the conditional  $\hat{\pi}_{Y|X=x}(y)$  using Langevin dynamics. The score estimator for the conditional distribution is,

$$\begin{aligned} \nabla_y \log \hat{\pi}_{Y|X=x}(y) &= \nabla_y [\log(M(V(x, y; \varphi_{\theta^*}, \psi_{\theta^*}))\sigma(x)\tau(y)) - \log(\sigma(x))] \\ &\approx \nabla_y \log(M(V(x, y; \varphi_{\theta^*}, \psi_{\theta^*}))) + s_\theta(y). \end{aligned}$$

We therefore approximate  $\nabla_y \hat{\pi}_{Y|X=x}(y)$  by directly differentiating  $\log M(V(x, y))$  using standard automatic differentiation tools and adding the result to an unconditional score estimate  $s_\theta(y)$ . The full Langevin sampling algorithm for general regularized optimal transport is shown in Algorithm 2.

We note that our method has the effect of biasing the Langevin iterates towards the region where  $\hat{\pi}_{Y|X=x}$  is localized. This may be beneficial for Langevin sampling, which enjoys exponentially fast mixing when sampling log-concave distributions. In the supplementary material, we prove a known result that for the entropy regularized problem given in Proposition 2.3: the compatibility  $M(V(x, y; \varphi^*, \psi^*)) = \frac{1}{e} \exp\left(\frac{1}{\lambda}(\varphi^*(x) + \psi^*(y) - c(x, y))\right)$  is log-concave with respect to  $y$ . For  $\lambda \rightarrow 0$ , this localizes around the optimal transport of  $x$ ,  $T(x)$ , and so heuristically should lead to faster mixing.

## 4 Theoretical Analysis

In principle, the empirical setting of Definition 2.1 poses an unconstrained optimization problem over  $\mathbb{R}^{|\mathcal{X}|} \times \mathbb{R}^{|\mathcal{Y}|}$ , which could be optimized directly by gradient descent on vectors  $(\varphi, \psi)$ . The

---

**Algorithm 1** Density Estimation.

**Input:** Step size  $\gamma$ , batch size  $m$   
**Input:** Nets  $\varphi_{\theta_1}, \psi_{\theta_2}$ .  
**Input:** Datasets  $\sigma, \tau$ . Time steps  $T > 0$ .  
**Output:** Trained  $\varphi_{\theta_1^*}, \psi_{\theta_2^*}$ .  
**for**  $t = 1 \dots T$ . **do**  
  Sample  $X_1, \dots, X_m \sim \sigma$ ,  
  and  $Y_1, \dots, Y_m \sim \tau$ .  
  Stochastic gradient update  $\varphi_{\theta_1}, \psi_{\theta_2}$ :  
   $\Delta_1 \leftarrow \sum_{i,j=1}^m \nabla_{\theta_1} [\varphi_{\theta_1}(X_i) - H^*(V(X_i, Y_j))]$ .  
   $\Delta_2 \leftarrow \sum_{i,j=1}^m \nabla_{\theta_2} [\psi_{\theta_2}(Y_j) - H^*(V(X_i, Y_j))]$ .  
   $\theta_1 \leftarrow \theta_1 + \gamma \Delta_1$ .  
   $\theta_2 \leftarrow \theta_2 + \gamma \Delta_2$ .  
**end for**  
**Output** parameters  $\{\theta_1, \theta_2\}$ .

---



---

**Algorithm 2** SCONES Sampling Procedure

**Input:** Noise levels  $\tau_1 > \dots > \tau_N$ .  
**Input:** Dual vars.  $\tilde{\varphi}(x), \tilde{\psi}(y)$ . Source  $x \in \mathcal{X}$ .  
**Input:** Time steps  $T > 0$ . Step size  $\epsilon > 0$ .  
**Output:** Data sample  $\tilde{y} \sim \pi_{Y|X=x}(y)$ .  
Initialize  $\tilde{y}_{1,0} \sim \mathcal{N}(0, I)$ .  
**for**  $\tau_i, i = 1 \dots N$  **do**  
  **for**  $t = 1 \dots T$ . **do**  
    Sample  $z \sim \mathcal{N}(0, \tau_i)$ .  
    Compute score update:  
     $\Delta_s \leftarrow s_{\theta}(\tilde{y}_{i,t-1})$ .  
     $\Delta_{\pi} \leftarrow \nabla_y \log M(V(x, \tilde{y}_{i,t-1}; \tilde{\varphi}, \tilde{\psi}))$ .  
     $\tilde{x}_{i,t} = \tilde{x}_{i,t-1} + (\epsilon/2)(\Delta_s + \Delta_{\pi}) + \sqrt{\epsilon}z$ .  
  **end for**  
  Initialize  $\tilde{x}_{i+1,0} = \tilde{x}_{i,T}$ .  
**end for**  
**Output** sample  $\tilde{x}_{N,T}$ .

---

point of a more expensive neural network parametrization  $\varphi_{\theta}, \psi_{\theta}$  is to learn a *continuous* distribution that agrees with the empirical optimal transport plan between discrete  $\sigma, \tau$ , and that generalizes to a continuous space containing  $\mathcal{X} \times \mathcal{Y}$ . By training  $\varphi_{\theta}, \psi_{\theta}$ , we approximate the underlying continuous data distribution up to optimization error and up to statistical estimation error between the empirical coupling and the population coupling. In the present section, we justify this approach by proving convergence of Algorithm 1 to the global maximizer of  $J_{\lambda}(\varphi, \psi)$ , under assumptions of large network width, along with a quantitative bound on optimization error. In Section B.1 of the Appendix, we provide a cursory analysis of rates of statistical estimation of entropy regularized Sinkhorn couplings. We make the following main assumptions on the neural networks  $\varphi_{\theta}$  and  $\psi_{\theta}$ .

**Assumption 4.1** (Approximate Linearity). Let  $f_{\theta}(x)$  be a neural network with parameters  $\theta \in \Theta$ , where  $\Theta$  is a set of feasible weights, for example those reachable by gradient descent. Fix a dataset  $\{X_i\}_{i=1}^N$  and let  $\mathcal{K}_{\theta} \in \mathbb{R}^{N \times N}$  be the Gram matrix of coordinates  $[\mathcal{K}_{\theta}]_{ij} = \langle \nabla_{\theta} f_{\theta}(X_i), \nabla_{\theta} f_{\theta}(X_j) \rangle$ . Then  $f_{\theta}(x)$  must satisfy,

1. There exists  $R \gg 0$  so that  $\Theta \subseteq B(0, R)$ , where  $B(0, R)$  is the Euclidean ball of radius  $R$ .
2. There exist  $\rho_M > \rho_m > 0$  such that for  $\theta \in \Theta$ ,  

$$\rho_M \geq \lambda_{\max}(\mathcal{K}_{\theta}) \geq \lambda_{\min}(\mathcal{K}_{\theta}) \geq \rho_m > 0.$$
3. For  $\theta \in \Theta$  and for all data points  $\{X_i\}_{i=1}^N$ , the Hessian matrix  $D_{\theta}^2 f_{\theta}(X_i)$  is bounded in spectral norm:  $\|D_{\theta}^2 f_{\theta}(X_i)\| \leq \frac{\rho_M}{C_h}$ , where  $C_h \gg 0$  depends only on  $R, N$ , and the regularization  $\lambda$ .

The dependencies of  $C_h$  are made clear in the Supplemental Materials, Section B. The quantity  $\mathcal{K}_{\theta}$  is called the *neural tangent kernel* (NTK) associated with the network  $f_{\theta}(x)$ . It has been shown for a variety of nets that, at sufficiently large width, the NTK is well conditioned and nearly constant on the set of weights reachable by gradient descent on a convex objective function [16, 6, 7]. For instance, fully-connected networks with smooth and Lipschitz-continuous activations fall into this class and hence satisfy Assumption 4.1 when the width of all layers is sufficiently large [16].

First, we show in Theorem 4.2 that when  $\varphi, \psi$  are parametrized by neural networks satisfying Assumption 4.1, gradient descent converges to *global* maximizers of the dual objective. This provides additional justification for the large-scale approach of Seguy et al. [22].

**Theorem 4.2** (Optimizing Neural Nets). *Suppose  $J_{\lambda}(\varphi, \psi)$  is  $\frac{1}{s}$ -strongly smooth in  $l_{\infty}$  norm. Let  $\varphi_{\theta}, \psi_{\theta}$  be neural networks satisfying Assumption 4.1 for the dataset  $\{(x_i, y_i)\}_{i=1}^N$ ,  $N = |\mathcal{X}| \cdot |\mathcal{Y}|$ .*

*Then gradient descent of  $J_{\lambda}(\varphi_{\theta}, \psi_{\theta})$  with respect to  $\theta$  at learning rate  $\eta = \frac{\lambda}{2\rho_M}$  converges to an  $\epsilon$ -approximate global maximizer of  $J_{\lambda}$  in at most  $\left(\frac{2\kappa R^2}{s}\right) \epsilon^{-1}$  iterations, where  $\kappa = \frac{\rho_M}{\rho_m}$ .*

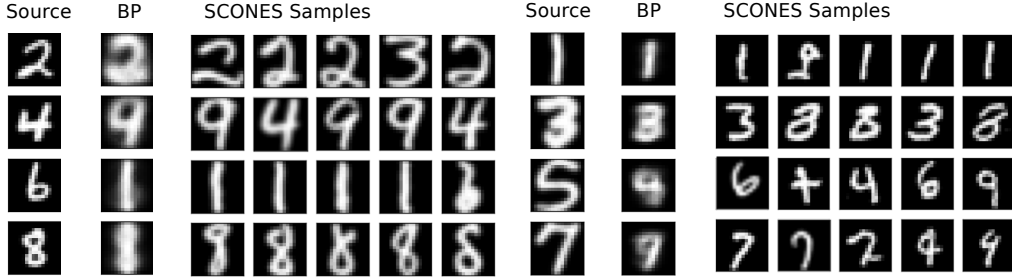


Figure 3: Comparison of Barycentric Projection [22] to SCONES for optimal transport between USPS and MNIST datasets of handwritten digits. (Left) Transporting MNIST to USPS. (Right) Transporting USPS to MNIST. Here, we show transportation of the  $\chi^2$  regularized problem at  $\lambda = 0.001$ .

Given outputs  $\hat{\varphi}, \hat{\psi}$  of Algorithm 1, we may assume by Theorem 4.2 that the networks are  $\epsilon$ -approximate global maximizers of  $J_\lambda(\varphi, \psi)$ . Due to  $\lambda\alpha$ -strong convexity of the primal objective, the optimization error  $\epsilon$  bounds the distance of the underlying pseudo-plan  $\hat{\pi}$  from the true global extrema. We make this bound concrete in Theorem 4.3, which guarantees that approximately maximizing  $J_\lambda(\varphi, \psi)$  is sufficient to produce a close approximation of the true empirical Sinkhorn coupling.

**Theorem 4.3** (Stability of the OT Problem). *Suppose  $K_\lambda(\pi)$  is  $s$ -strongly convex in  $l_1$  norm and let  $\mathcal{L}(\varphi, \psi, \pi)$  be the Lagrangian of the regularized optimal transport problem. For  $\hat{\varphi}, \hat{\psi}$  which are  $\epsilon$ -approximate maximizers of  $J_\lambda(\varphi, \psi)$ , the pseudo-plan  $\hat{\pi} = M_f(V(x, y; \hat{\varphi}, \hat{\psi}))\sigma(x)\tau(y)$  satisfies*

$$|\hat{\pi} - \pi^*|_1 \leq \sqrt{\frac{2\epsilon}{s}} \leq \frac{1}{s} \left| \nabla_{\hat{\pi}} \mathcal{L}(\hat{\varphi}, \hat{\psi}, \hat{\pi}) \right|_1.$$

Theorem 4.3 guarantees that if one can approximately optimize the dual objective using Algorithm 1, then the corresponding coupling  $\hat{\pi}$  is close in  $l_1$  norm to the true optimal transport coupling. This approximation guarantee justifies the choice to draw samples  $\tilde{\pi}_{Y|X=x}$  as an approximation to sampling  $\pi_{Y|X=x}$  instead. Both Theorems 4.2 and 4.3 are proven in Section B of the Appendix.

## 5 Experiments

Our main point of comparison is the barycentric projection method proposed by Seguy et al. [22], which trains a neural network  $T_\theta : \mathcal{X} \rightarrow \mathcal{Y}$  to map source data to target data by optimizing the objective  $\theta := \arg \min_\theta \mathbb{E}_{\pi_{Y|X=x}} [|T_\theta(x) - Y|^2]$ . For transportation experiments between USPS [19] and MNIST [13] datasets, we scale both datasets to 16px and parametrize the dual variables and barycentric projections by fully connected ReLU networks. We train score estimators for MNIST and USPS at 16px resolution using the method and architecture of [24]. For transportation experiments using CelebA [17], dual variables  $\varphi, \psi$  are parametrized as ReLU FCNs with 8, 2048-dimensional hidden layers. Both the barycentric projection and the score estimators use the U-Net based image-to-image architecture introduced in [24]. Numerical hyperparameters like learning rates, optimizer parameters, and annealing schedules, along with additional details of our neural network architectures, are tabulated in Section C of the Appendix.

### 5.1 Optimal Transportation of Image Data

We show in Figure 3 a qualitative plot of SCONES samples on transportation between MNIST and USPS digits. We also show in Section 1, Figure 1 a qualitative plot of transportation of CelebA images. Because barycentric projection averages  $\pi_{Y|X=x}$ , output images are blurred and show visible mixing of multiple digits. By directly sampling the optimal transport plan, SCONES can separate these modes and generate more realistic images.

At low regularization levels, Algorithm 1 becomes more expensive and can become numerically unstable. As shown in Figures 3 and 1, SCONES can be used to sample the Sinkhorn coupling in intermediate regularization regimes, where optimal transport has a nontrivial effect despite  $\pi_{Y|X=x}$  not concentrating on a single image.

	KL regularization,			$\chi^2$ regularization,		
	$\lambda = 0.1$	$\lambda = 0.01$	$\lambda = 0.005$	$\lambda = 0.1$	$\lambda = 0.01$	$\lambda = 0.001$
SCONES, Super-res.	35.59	35.77	43.80	25.84	25.64	25.59
Bary. Proj., Super-res.	193.92	230.85	228.78	190.10	216.54	212.72
SCONES, Identity	36.62	34.84	43.99	25.51	25.65	27.88
Bary. Proj., Identity	195.64	217.24	217.67	188.29	219.96	214.90

Table 1: FID metric of samples generated by barycentric projection and SCONES, computed on  $n = 5000$  samples from each model. For comparison to unregularized OT methods, we also trained a Wasserstein-2 GAN ( $W_2$  GAN) [14] and a Wasserstein-2 Generative Network ( $W_2$  Gen) [11].  $W_2$  GAN achieves FIDs 55.77 on the super-res. task and 32.617 on the identity task.  $W_2$  Gen achieves FIDs 32.80 on the super-res. task and 20.57 on the identity task.

To quantitatively assess the quality of images generated by SCONES, we compute the FID scores of generated CelebA images on two optimal transport problems: transporting 2x down-sampled CelebA images to CelebA (the ‘Super-res.’ task) and transporting CelebA to CelebA (the ‘Identity’ task) for a variety of regularization parameters. The FID score is a popular measurement of sample quality for image generative models and it is a proxy for agreement between the distribution of SCONES samples of the marginal  $\pi_Y(y)$  and the true distribution  $\tau(y)$ . In both cases, we partition CelebA into two datasets of equal size and optimize Algorithm 1 using separated partitions as source and target data, resizing the source data in the super-resolution task. As shown in Table 1, SCONES has a significantly lower FID score than samples generated by barycentric projection. However, under ideal tuning, the unconditional score network generates CelebA samples with FID score 10.23 [24], so there is some cost in sample quality incurred when using SCONES.

## 5.2 Sampling Synthetic Data

To compare SCONES to a ground truth Sinkhorn coupling in a continuous setting, we consider entropy regularized optimal transport between Gaussian measures on  $\mathbb{R}^d$ . Given  $\sigma = \mathcal{N}(\mu_1, \Sigma_1)$  and  $\tau = \mathcal{N}(\mu_2, \Sigma_2)$ , the Sinkhorn coupling of  $\sigma, \tau$  is itself a Gaussian measure and it can be written in closed form in terms of the regularization  $\lambda$  and the means and covariances of  $\sigma, \tau$  [8]. In dimensions  $d \in \{2, 16, 54, 128, 256\}$ , we consider  $\Sigma_1, \Sigma_2$  whose eigenvectors are uniform random (i.e. drawn from the Haar measure on  $SO(d)$ ) and whose eigenvalues are sampled uniform i.i.d.

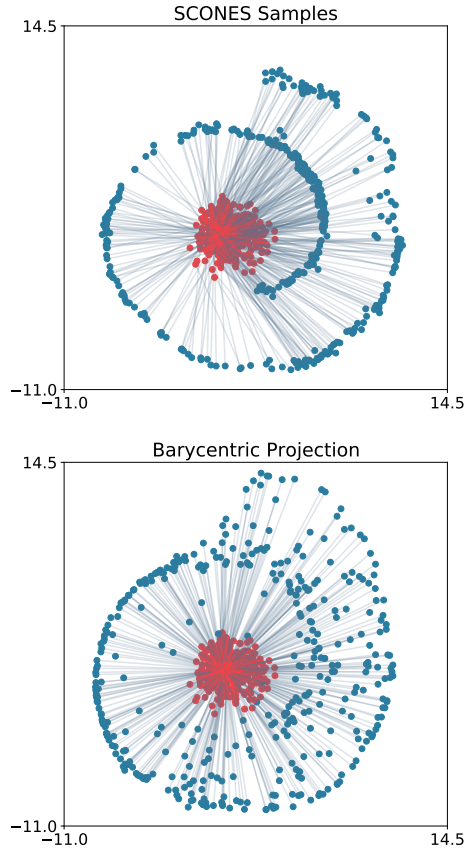


Figure 4: Entropy regularized,  $\lambda = 2$ ,  $L^2$  cost SCONES and BP samples on transportation from a unit Gaussian source distribution to the Swiss Roll target distribution. For many samples, the Barycentric average lies off the manifold of high target density, whereas SCONES can separate multiple modes of the conditional coupling and correctly recover the target distribution.



	$d = 2$	$d = 16$	$d = 64$	$d = 128$	$d = 256$
SCONES	$0.025 \pm 0.0014$	$0.52 \pm 0.0086$	$1.2 \pm 0.014$	$1.4 \pm 0.066$	$2.0 \pm 0.047$
BP	$7.1 \pm 0.13$	$35 \pm 0.23$	$42 \pm 0.14$	$41 \pm 0.088$	$41 \pm 0.098$

Table 2: Comparison of SCONES to BP on KL-regularized optimal transport between random high-dimensional Gaussians. In each cell, we report the average BW-UVP between a sample empirical covariance and the analytical solution. We report the average over  $n = 10$  independent random source, target Gaussians and the standard error of the mean.

from  $[1, 10]$ . In all cases, we set means  $\mu_1, \mu_2$  equal to zero and choose regularization  $\lambda = 2d$ . In the Gaussian setting,  $\mathbb{E}[\|x - y\|_2^2]$  is of order  $d$ , so this choice of scaling ensures a fair comparison across problem dimensions by fixing the relative magnitudes of the cost and regularization terms.

We evaluate performance on this task using the Bures-Wasserstein Unexplained Variance Percentage [4],  $\text{BW-UV}(\hat{\pi}, \pi^\lambda)$ , where  $\pi^\lambda$  is the closed form solution given by Janati et al. [8] and where  $\hat{\pi}$  is the joint empirical covariance of  $k = 10000$  samples  $(x, y) \sim \pi$  generated using either SCONES or Barycentric Projection. We train SCONES according to Algorithm 1 and generate samples according to Algorithm 2. In place of a score estimate, we use the ground truth target score  $\nabla_y \log \tau(y) = \Sigma_2^{-1}(y - \mu_2)$  and omit annealing. We compare SCONES samples to the true solution in the BW-UVP metric [4] which is measured on a scale from 0 to 100, lower is better. We report  $\text{BW-UV}(\hat{\pi}, \pi^\lambda)$  where  $\hat{\pi}$  is a  $2d$ -by- $2d$  joint empirical covariance of SCONES samples  $(x, y) \sim \hat{\pi}$  or of BP samples  $(x, T_\theta(x))$ ,  $x \sim \sigma$  and  $\pi^\lambda$  is the closed-form covariance.

## 6 Discussion and Future Work

We introduce and analyze the SCONES method for learning and sampling large-scale optimal transport plans. Our method takes the form of a conditional sampling problem for which the conditional score decomposes naturally into a prior, unconditional score  $\nabla_y \log \tau(y)$  and a ‘‘compatibility term’’  $\nabla_y \log M(V(x, y))$ . This decomposition illustrates a key benefit of SCONES: one score network may re-used to cheaply transport many source distributions to the same target. In contrast, learned forward-model-based transportation maps require an expensive training procedure for each distinct pair of source and target distribution. This benefit comes in exchange of increased computational cost of iterative sampling. For example, generating 1000 samples requires roughly 3 hours using one NVIDIA 2080 Ti GPU. The cost to sample score-based models may fall with future engineering advances, but iterative sampling intrinsically require multiple forward pass evaluations of the score estimator as opposed to a single evaluation of a learned transportation mapping.

There is much future work to be done. First, we study only simple fully connected ReLU networks as parametrizations of the dual variables. Interestingly, we observe that under  $L^2$  transportation cost, parametrization by multi-layer convolutional networks perform equally or worse than their FCN counterparts when optimizing Algorithm 1. One explanation may be the *permutation invariance* of  $L^2$  cost: applying a permutation of coordinates to the source and target distribution does not change the optimal objective value and the optimal coupling is simply conjugated by a coordinate permutation. As a consequence, the optimal coupling may depend non-locally on input data coordinates, violating the inductive biases of localized convolutional filters. Understanding which network parametrizations or inductive biases are best for a particular choice of transportation cost, source distribution, and target distribution, is one direction for future investigation.

Second, it remains to explore whether there is a potential synergistic effect between Langevin sampling and optimal transport. Heuristically, as  $\lambda \rightarrow 0$  the conditional plan  $\pi_{Y|X=x}$  concentrates around the transport image of  $x$ , which should improve the mixing time required by Langevin dynamics to explore high density regions of space. In Section B of the Appendix, we prove a known result, that the entropy regularized  $L^2$  cost compatibility term  $M(V(x, y)) = e^{V(x, y)/\lambda}$  is a log-concave function of  $y$  for fixed  $x$ . If the target distribution is itself log-concave, the conditional coupling  $\pi_{Y|X=x}$  is also log-concave and hence Langevin sampling enjoys exponentially fast mixing time. However, more work is required to understand the impacts of non-log-concavity of the target and of optimization errors when learning the compatibility and score functions in practice. We look forward to future developments on these and other aspects of large-scale regularized optimal transport.

## Acknowledgments and Disclosure of Funding

M.D. acknowledges funding from Northeastern University’s Undergraduate Research & Fellowships office and the Goldwater Award. P.H. was supported in part by NSF awards 2053448, 2022205, and 1848087.

## References

- [1] Jean-David Benamou and Mélanie Martinet. Capacity constrained entropic optimal transport, sinkhorn saturated domain out-summation and vanishing temperature. 2020.
- [2] Mathieu Blondel, Vivien Seguy, and Antoine Rolet. Smooth and sparse optimal transport. In Amos Storkey and Fernando Perez-Cruz, editors, *Proceedings of the Twenty-First International Conference on Artificial Intelligence and Statistics*, volume 84 of *Proceedings of Machine Learning Research*, page 880–889. PMLR, Apr 2018. URL <http://proceedings.mlr.press/v84/blondel18a.html>.
- [3] S. Boyd, S.P. Boyd, L. Vandenberghe, and Cambridge University Press. *Convex Optimization*. Berichte über verteilte messsysteme. Cambridge University Press, 2004. ISBN 978-0-521-83378-3. URL <https://books.google.com/books?id=mYm0bLd3fcoC>.
- [4] Yongxin Chen, Jiaojiao Fan, and Amirhossein Taghvaei. Scalable computations of wasserstein barycenter via input convex neural networks. In Marina Meila and Tong Zhang, editors, *Proceedings of the 38th International Conference on Machine Learning*, volume 139 of *Proceedings of Machine Learning Research*, pages 1571–1581. PMLR, 18–24 Jul 2021. URL <https://proceedings.mlr.press/v139/chen21e.html>.
- [5] Marco Cuturi. Sinkhorn distances: Lightspeed computation of optimal transport. In C. J. C. Burges, L. Bottou, M. Welling, Z. Ghahramani, and K. Q. Weinberger, editors, *Advances in Neural Information Processing Systems*, volume 26. Curran Associates, Inc., 2013. URL <https://proceedings.neurips.cc/paper/2013/file/af21d0c97db2e27e13572cbf59eb343d-Paper.pdf>.
- [6] Simon Du and Wei Hu. Width provably matters in optimization for deep linear neural networks. In Kamalika Chaudhuri and Ruslan Salakhutdinov, editors, *Proceedings of the 36th International Conference on Machine Learning*, volume 97 of *Proceedings of Machine Learning Research*, page 1655–1664. PMLR, Jun 2019. URL <http://proceedings.mlr.press/v97/du19a.html>.
- [7] Simon Du, Jason Lee, Haochuan Li, Liwei Wang, and Xiyu Zhai. Gradient descent finds global minima of deep neural networks. In Kamalika Chaudhuri and Ruslan Salakhutdinov, editors, *Proceedings of the 36th International Conference on Machine Learning*, volume 97 of *Proceedings of Machine Learning Research*, page 1675–1685. PMLR, Jun 2019. URL <http://proceedings.mlr.press/v97/du19c.html>.
- [8] Hicham Janati, Boris Muzellec, Gabriel Peyré, and Marco Cuturi. Entropic optimal transport between unbalanced gaussian measures has a closed form. In *Neurips 2020*, 2020.
- [9] Alexia Jolicoeur-Martineau, Rémi Piché-Taillefer, Ioannis Mitliagkas, and Remi Tachet des Combes. Adversarial score matching and improved sampling for image generation. In *International Conference on Learning Representations*, 2021. URL <https://openreview.net/forum?id=eLfqMl3z3lq>.
- [10] Sham M Kakade, Shai Shalev-Shwartz, and Ambuj Tewari. On the duality of strong convexity and strong smoothness: Learning applications and matrix regularization. page 10.
- [11] Alexander Korotin, Vage Egiazarian, Arip Asadulaev, Alexander Safin, and Evgeny Burnaev. Wasserstein-2 generative networks. In *International Conference on Learning Representations*, 2021. URL [https://openreview.net/forum?id=bEoxzW\\_EXsa](https://openreview.net/forum?id=bEoxzW_EXsa).
- [12] Wouter M. Kouw and Marco Loog. An introduction to domain adaptation and transfer learning. *arXiv:1812.11806 [cs, stat]*, Jan 2019. URL <http://arxiv.org/abs/1812.11806>. arXiv: 1812.11806.

- [13] Yann LeCun, Corinna Cortes, and CJ Burges. Mnist handwritten digit database. *ATT Labs [Online]*. Available: <http://yann.lecun.com/exdb/mnist>, 2, 2010.
- [14] Jacob Leygonie, Jennifer She, Amjad Almahairi, Sai Rajeswar, and Aaron Courville. Adversarial computation of optimal transport maps, 2019.
- [15] Lingxiao Li, Aude Genevay, Mikhail Yurochkin, and Justin M Solomon. Continuous regularized wasserstein barycenters. In H. Larochelle, M. Ranzato, R. Hadsell, M. F. Balcan, and H. Lin, editors, *Advances in Neural Information Processing Systems*, volume 33, page 17755–17765. Curran Associates, Inc., 2020. URL <https://proceedings.neurips.cc/paper/2020/file/cdf1035c34ec380218a8cc9a43d438f9-Paper.pdf>.
- [16] Chaoyue Liu, Libin Zhu, and Misha Belkin. On the linearity of large non-linear models: when and why the tangent kernel is constant. In H. Larochelle, M. Ranzato, R. Hadsell, M. F. Balcan, and H. Lin, editors, *Advances in Neural Information Processing Systems*, volume 33, page 15954–15964. Curran Associates, Inc., 2020. URL <https://proceedings.neurips.cc/paper/2020/file/b7ae8fecf15b8b6c3c69ecea636d203-Paper.pdf>.
- [17] Ziwei Liu, Ping Luo, Xiaogang Wang, and Xiaoou Tang. Deep learning face attributes in the wild. In *Proceedings of International Conference on Computer Vision (ICCV)*, December 2015.
- [18] Giulia Luise, Saverio Salzo, Massimiliano Pontil, and Carlo Ciliberto. Sinkhorn barycenters with free support via frank-wolfe algorithm. In H. Wallach, H. Larochelle, A. Beygelzimer, F. d’Alché-Buc, E. Fox, and R. Garnett, editors, *Advances in Neural Information Processing Systems*, volume 32, page 9322–9333. Curran Associates, Inc., 2019. URL <https://proceedings.neurips.cc/paper/2019/file/9f96f36b7aae3b1ff847c26ac94c604e-Paper.pdf>.
- [19] O. Matan, R. Kiang, C. E. Stenard, B. E. Boser, J. Denker, J. Denker, D. Henderson, R. Howard, W. Hubbard, L. Jackel, and et al. *Handwritten character recognition using neural network architectures*. 1990. URL [/paper/Handwritten-character-recognition-using-neural-Matan-Kiang/8f2b909fa1aad7e9f13603d721ff953325a4f97d](https://proceedings.neurips.cc/paper/Handwritten-character-recognition-using-neural-Matan-Kiang/8f2b909fa1aad7e9f13603d721ff953325a4f97d).
- [20] James Melbourne. Strongly convex divergences. *Entropy*, 22(1111):1327, Nov 2020. doi: 10.3390/e22111327.
- [21] Sebastian Nowozin, Botond Cseke, and Ryota Tomioka. f-gan: Training generative neural samplers using variational divergence minimization. *Advances in Neural Information Processing Systems*, 29, 2016. URL <https://proceedings.neurips.cc/paper/2016/hash/cedebb6e872f539bef8c3f919874e9d7-Abstract.html>.
- [22] Vivien Seguy, Bharath Bhushan Damodaran, Remi Flamary, Nicolas Courty, Antoine Rolet, and Mathieu Blondel. Large scale optimal transport and mapping estimation. In *International Conference on Learning Representations*, 2018. URL <https://openreview.net/forum?id=B1z1p1bRW>.
- [23] Richard Sinkhorn. A relationship between arbitrary positive matrices and stochastic matrices. *Canadian Journal of Mathematics*, 18:303–306, 1966. ISSN 0008-414X, 1496-4279. doi: 10.4153/CJM-1966-033-9.
- [24] Yang Song and Stefano Ermon. Improved techniques for training score-based generative models. In Hugo Larochelle, Marc’ Aurelio Ranzato, Raia Hadsell, Maria-Florina Balcan, and Hsuan-Tien Lin, editors, *Advances in Neural Information Processing Systems 33: Annual Conference on Neural Information Processing Systems 2020, NeurIPS 2020, December 6-12, 2020, virtual*, 2020.
- [25] Matthew Thorpe. Introduction to optimal transport. page 56.
- [26] C. Villani. *Topics in Optimal Transportation*. Graduate studies in mathematics. American Mathematical Society, 2003. ISBN 978-0-8218-3312-4. URL [https://books.google.com/books?id=R\\_nWqjq89oEC](https://books.google.com/books?id=R_nWqjq89oEC).

## A Regularizing Optimal Transport with $f$ -Divergences

Name	$f(v)$	$f^*(v)$	$f^{*'}$	$\text{Dom}(f^*(v))$
Kullback-Leibler	$v \log(v)$	$\exp(v - 1)$	$\exp(v - 1)$	$v \in \mathbb{R}$
Reverse KL	$-\log(v)$	$\log(-\frac{1}{v}) - 1$	$-\frac{1}{v}$	$v < 0$
Pearson $\chi^2$	$(v - 1)^2$	$\frac{v^2}{4} + v$	$\frac{v}{2} + 1$	$v \in \mathbb{R}$
Squared Hellinger	$(\sqrt{v} - 1)^2$	$\frac{v}{1-v}$	$(1 - v)^{-2}$	$v < 1$
Jensen-Shannon	$-(v + 1) \log(\frac{1+v}{2}) + v \log v$	$\frac{e^x}{2 - e^x}$	$\frac{2x}{e^x - 2} + x - \log(2 - e^x)$	$v < \log(2)$
GAN	$v \log(v) - (v + 1) \log(v + 1)$	$-v - \log(e^{-v} - 1)$	$(e^{-v} - 1)^{-1}$	$v < 0$

Table 3: A list of  $f$ -Divergences, their Fenchel-Legendre conjugates, and the derivative of their conjugates. These functions determine the corresponding dual regularizers  $H_f^*(v)$  and compatibility functions  $M_f(v)$ . We take definitions of each divergence from [21]. Note that there are many equivalent formulations as each  $f(v)$  is defined only up to additive  $c(v - 1)$ ,  $c \in \mathbb{R}$ , and the resulting optimization problems are defined only up to shifting and scaling the objective.

Here are some general properties of  $f$ -Divergences which are also used in Section B. We provide examples of  $f$ -Divergences in Table 3. The specific forms of  $H_f^*(v)$  and  $M_f(v)$  are determined by  $f(v)$ ,  $f^*(v)$ , and  $f^{*'}(v)$ , which can in turn be used to formulate Algorithms 1 and 2 for each divergence.

**Definition A.1** ( $f$ -Divergences). Let  $f : \mathbb{R} \rightarrow \mathbb{R}$  be convex with  $f(1) = 0$  and let  $p, q$  be probability measures such that  $p$  is absolutely continuous with respect to  $q$ . The corresponding  $f$ -Divergence is defined  $D_f(p||q) = \mathbb{E}_q[f(\frac{dp(x)}{dq(x)})]$  where  $\frac{dp(x)}{dq(x)}$  is the Radon-Nikodym derivative of  $p$  w.r.t.  $q$ .

**Proposition A.2** (Strong Convexity of  $D_f$ ). Let  $\mathcal{X}$  be a countable compact metric space. Fix  $q \in \mathcal{M}_+(\mathcal{X})$  and let  $\mathcal{P}_q(\mathcal{X})$  be the set of probability measures on  $\mathcal{X}$  that are absolutely continuous with respect to  $q$  and which have bounded density over  $\mathcal{X}$ . Let  $f : \mathbb{R} \rightarrow \mathbb{R}$  be  $\alpha$ -strongly convex with corresponding  $f$ -Divergence  $D_f(p||q)$ . Then, the function  $H_f(p) := D_f(p||q)$  defined over  $p \in \mathcal{P}_q(\mathcal{X})$  is  $\alpha$ -strongly convex in 1-norm: for  $p_0, p_1 \in \mathcal{P}_q(\mathcal{X})$ ,

$$H_f(p_1) \geq H_f(p_0) + \langle \nabla_p H_f(p_0), p_1 - p_0 \rangle + \frac{\alpha}{2} |p_1 - p_0|_1^2. \quad (2)$$

*Proof.* Define the measure  $p_t = tp_1 + (1 - t)p_0$ . Then  $H_f$  satisfies the following convexity inequality (Melbourne [20], Proposition 2).

$$H_f(p_t) \leq tH_f(p_1) + (1 - t)H_f(p_0) - \alpha (t|p_1 - p_t|_{\text{TV}}^2 + (1 - t)|p_0 - p_t|_{\text{TV}}^2)$$

By assumption that  $\mathcal{X}$  is countable,  $|p - q|_{\text{TV}} = \frac{1}{2}|p - q|_1$ . It follows that,

$$\begin{aligned} H_f(p_1) &\geq H_f(p_0) + \frac{H_f(p_0 + t(p_1 - p_0)) - H_f(p_0)}{t} + \frac{\alpha}{2} (|p_1 - p_t|_1^2 + (t^{-1} - 1)|p_0 - p_t|_1^2) \\ &\geq H_f(p_0) + \frac{H_f(p_0 + t(p_1 - p_0)) - H_f(p_0)}{t} + \frac{\alpha}{2} |p_1 - p_t|_1^2 \end{aligned}$$

and, taking the limit  $t \rightarrow 0$ , the inequality (2) follows.  $\square$

For the purposes of solving empirical regularized optimal transport, the technical conditions of Proposition A.2 hold. Additionally, note that  $\alpha$ -strong convexity of  $f$  is sufficient but not necessary for strong convexity of  $H_f$ . For example, entropy regularization uses  $f_{\text{KL}}(v) = v \log(v)$  which is not strongly convex over its domain,  $\mathbb{R}_+$ , but which yields a regularizer  $H_{\text{KL}}(p) = \text{KL}(p||q)$  that is 1-strongly convex in  $l_1$  norm when  $q$  is uniform. This follows from Pinsker's inequality as shown in [22]. Also, if  $f$  is  $\alpha$ -strongly convex over a subinterval  $[a, b]$  of its domain, then Proposition A.2 holds under the additional assumption that  $a \leq \frac{dp(x)}{dq(x)}(x) \leq b$  uniformly over  $x \in \mathcal{X}$ .

## B Proofs

For convenience, we repeat the main assumptions and statements of theorems alongside their proofs. First, we prove the following properties about  $f$ -divergences.

**Proposition, 2.4** – Regularization with  $f$ -Divergences. *Consider the empirical setting of Definition 2.1. Let  $f(v) : \mathbb{R} \rightarrow \mathbb{R}$  be a differentiable  $\alpha$ -strongly convex function with convex conjugate  $f^*(v)$ . Set  $f^{*'}(v) = \partial_v f^*(v)$ . Define the violation function  $V(x, y; \varphi, \psi) = \varphi(x) + \psi(y) - c(x, y)$ . Then,*

1. *The  $D_f$  regularized primal problem  $K_\lambda(\pi)$  is  $\lambda\alpha$ -strongly convex in  $l_1$  norm. With respect to dual variables  $\varphi \in \mathbb{R}^{|\mathcal{X}|}$  and  $\psi \in \mathbb{R}^{|\mathcal{Y}|}$ , the dual problem  $J_\lambda(\varphi, \psi)$  is concave, unconstrained, and  $\frac{1}{\lambda\alpha}$ -strongly smooth in  $l_\infty$  norm. Strong duality holds:  $K_\lambda(\pi) \geq J_\lambda(\varphi, \psi)$  for all  $\pi, \varphi, \psi$ , with equality for some triple  $\pi^*, \varphi^*, \psi^*$ .*
2.  *$J_\lambda(\varphi, \psi)$  takes the form*

$$J_\lambda(\varphi, \psi) = \mathbb{E}_\sigma[\varphi(x)] + \mathbb{E}_\tau[\psi(y)] - \mathbb{E}_{\sigma \times \tau}[H_f^*(V(x, y; \varphi, \psi))]$$

where  $H_f^*(v) = \lambda f^*(\lambda^{-1}v)$ .

3. *The optimal solutions  $(\pi^*, \varphi^*, \psi^*)$  satisfy*

$$\pi^*(x, y) = M_f(V(x, y; \varphi, \psi))\sigma(x)\tau(y)$$

where  $M_f(x, y) = f^{*'}(\lambda^{-1}v)$ .

*Proof.* By assumption that  $f$  is differentiable,  $K_\lambda(\pi)$  is continuous and differentiable with respect to  $\pi \in \mathcal{M}_+(\mathcal{X} \times \mathcal{Y})$ . By Proposition A.2, it is  $\lambda\alpha$ -strongly convex in  $l_1$  norm. By the Fenchel-Moreau theorem,  $K_\lambda(\pi)$  therefore has a unique minimizer  $\pi^*$  satisfying strong duality, and by [10, Theorem 6], the dual problem is  $\frac{1}{\lambda\alpha}$ -strongly smooth in  $l_\infty$  norm.

The primal and dual are related by the Lagrangian  $\mathcal{L}(\pi, \varphi, \psi)$ ,

$$\mathcal{L}(\varphi, \psi, \pi) = \mathbb{E}_\pi[c(x, y)] + \lambda H_f(\pi) + \mathbb{E}_\sigma[\varphi(x)] - \mathbb{E}_\pi[\varphi(x)] + \mathbb{E}_\tau[\varphi(y)] - \mathbb{E}_\pi[\psi(y)] \quad (3)$$

which has  $K_\lambda(\pi) = \max_{\varphi, \psi} \mathcal{L}(\varphi, \psi, \pi)$  and  $J_\lambda(\varphi, \psi) = \min_\pi \mathcal{L}(\varphi, \psi, \pi)$ . In the empirical setting,  $\pi, \sigma, \tau$  may be written as finite dimensional vectors with coordinates  $\pi_{x,y}, \sigma_x, \tau_y$  for  $x, y \in \mathcal{X} \times \mathcal{Y}$ . Minimizing the  $\pi$  terms of  $J_\lambda$ ,

$$\begin{aligned} & \min_{\pi \in \mathcal{M}(\mathcal{X} \times \mathcal{Y})} \left\{ \mathbb{E}_\pi[c(x, y) - \varphi(x) - \psi(y)] + \lambda \mathbb{E}_{\sigma \times \tau} \left[ f \left( \frac{d\pi(x, y)}{d\sigma(x)d\tau(y)} \right) \right] \right\} \\ &= \sum_{x, y \in \mathcal{X} \times \mathcal{Y}} - \max_{\pi_{x,y} \geq 0} \left\{ \pi_{x,y} \cdot (\varphi(x) + \psi(y) - c(x, y)) - \lambda \sigma_x \tau_y f \left( \frac{\pi_{x,y}}{\sigma_x \tau_y} \right) \right\} \\ &= \sum_{x, y \in \mathcal{X} \times \mathcal{Y}} -h_{x,y}^*(\varphi(x) + \psi(y) - c(x, y)) \end{aligned}$$

where  $h_{x,y}^*$  is the convex conjugate of  $(\lambda \sigma_x \tau_y) \cdot f(p/(\sigma_x \tau_y))$  w.r.t. the argument  $p$ . For general convex  $f(p)$ , it is true that  $[\lambda f(p)]^*(v) = \lambda f^*(\lambda^{-1}v)$  [3, Chapter 3]. Applying twice,

$$[(\lambda \sigma_x \tau_y) \cdot f(p/(\sigma_x \tau_y))]^*(v) = \lambda [(\sigma_x \tau_y) f(p/(\sigma_x \tau_y))]^*(\lambda^{-1}v) = (\lambda \sigma_x \tau_y) \cdot f^*(v/\lambda)$$

so that

$$\begin{aligned} & \min_{\pi \in \mathcal{M}_+(\mathcal{X} \times \mathcal{Y})} \mathbb{E}_\pi[c(x, y) - \varphi(x) - \psi(y)] + \lambda \mathbb{E}_{\sigma \times \tau} \left[ f \left( \frac{d\pi(x, y)}{d\sigma(x)d\tau(y)} \right) \right] \\ &= \sum_{x, y \in \mathcal{X} \times \mathcal{Y}} \sigma_x \tau_y \lambda f^*(\lambda^{-1}v) \\ &= - \mathbb{E}_{\sigma \times \tau}[H_f^*(V(x, y; \varphi, \psi))] \end{aligned}$$

for  $H_f^*(v) = \lambda f^*(\lambda^{-1}v)$ . The claimed form of  $J_\lambda(\varphi, \psi)$  follows.

Additionally, for general convex  $f(p)$ , it is true that  $\partial_v f^*(v) = \arg \max_p \{ \langle v, p \rangle - f(p) \}$ , [3, Chapter 3]. For  $\varphi^*, \psi^*$  maximizing  $J_\lambda(\varphi, \psi)$ , it follows by strong duality that

$$\begin{aligned} \pi_{x,y}^* &= \arg \min_{\pi \in \mathcal{M}_+(\mathcal{X} \times \mathcal{Y})} \mathcal{L}(\varphi^*, \psi^*, \pi) \\ &= \nabla_V \mathbb{E}_{\sigma \times \tau} [H_f^*(V(x, y; \varphi^*, \psi^*))] = M_f(V(x, y; \varphi^*, \psi^*)) \sigma_x \tau_y. \end{aligned}$$

as claimed.  $\square$

We proceed to proofs of the theorems stated in Section 4.

**Assumption, 4.1 – Approximate Linearity.** Let  $f_\theta(x)$  be a neural network with parameters  $\theta \in \Theta$ , where  $\Theta$  is a set of feasible weights, for example those reachable by gradient descent. Fix a dataset  $\{X_i\}_{i=1}^N$  and let  $\mathcal{K}_\theta \in \mathbb{R}^{N \times N}$  be the Gram matrix of coordinates  $[\mathcal{K}_\theta]_{ij} = \langle \nabla_\theta f_\theta(X_i), \nabla_\theta f_\theta(X_j) \rangle$ . Then  $f_\theta(x)$  must satisfy,

1. There exists  $R \gg 0$  so that  $\Theta \subseteq B(0, R)$ , where  $B(0, R)$  is the Euclidean ball of radius  $R$ .
2. There exist  $\rho_M > \rho_m > 0$  such that for  $\theta \in \Theta$ ,

$$\rho_M \geq \lambda_{\max}(\mathcal{K}_\theta) \geq \lambda_{\min}(\mathcal{K}_\theta) \geq \rho_m > 0.$$

3. For  $\theta \in \Theta$  and for all data points  $\{X_i\}_{i=1}^N$ , the Hessian matrix  $D_\theta^2 f_\theta(x_i)$  is bounded in spectral norm:

$$\|D_\theta^2 f_\theta(x_i)\| \leq \frac{\rho_M}{C_h}$$

where  $C_h \gg 0$  depends only on  $R, N$ , and the regularization  $\lambda$ .

The constant  $C_h$  may depend on the dataset size  $N$ , the upper bound of  $\rho_M$  for eigenvalues of the NTK, the regularization parameter  $\lambda$ , and it may also depend indirectly on the bound  $R$ .

**Theorem, 4.2 – Optimizing Neural Nets.** Suppose  $J_\lambda(\varphi, \psi)$  is  $\frac{1}{s}$ -strongly smooth in  $l_\infty$  norm. Let  $\varphi_\theta, \psi_\theta$  be neural networks satisfying Assumption 4.1 for the dataset  $\{(x_i, y_i)\}_{i=1}^N$ ,  $N = |\mathcal{X}| \cdot |\mathcal{Y}|$ .

Then gradient descent of  $J_\lambda(\varphi_\theta, \psi_\theta)$  with respect to  $\theta$  at learning rate  $\eta = \frac{\lambda}{2\rho_M}$  converges to an  $\epsilon$ -approximate global maximizer of  $J_\lambda$  in at most  $\left(\frac{2\kappa R^2}{s}\right) \epsilon^{-1}$  iterations, where  $\kappa = \frac{\rho_M}{\rho_m}$ .

*Proof.* For indices  $i$ , let  $S_{\theta_i} = (\varphi_{\theta_i}, \psi_{\theta_i})$  so that Assumption 4.1 applies with  $S_\theta$  in place of  $f_\theta$ .

**Lemma B.1 (Smoothness).**  $J_\lambda(S_\theta)$  is  $\frac{2\rho_M}{s}$ -strongly smooth in  $l_2$  norm with respect to  $\theta$ :

$$J_\lambda(S_{\theta_2}) \leq J_\lambda(S_{\theta_1}) + \langle \nabla_\theta J_\lambda(S_{\theta_1}), S_{\theta_2} - S_{\theta_1} \rangle + \frac{\rho_M}{\lambda} \|\theta_2 - \theta_1\|_2^2.$$

*Proof.* It is assumed that  $J_\lambda(S)$  is  $(\frac{1}{s}, l_\infty)$ -strongly smooth and that  $K_\lambda(\pi)$  is  $(s, l_1)$ -strongly convex. Note that  $(\frac{1}{s}, l_2)$ -strong smoothness is *weakest* in the sense that it is implied via norm equivalence by  $(\frac{1}{s}, l_q)$ -strong smoothness for  $2 \leq q \leq \infty$ .

$$\begin{aligned} J_\lambda(S_2) &\leq J_\lambda(S_1) + \langle \nabla_S J_\lambda(S_1), S_2 - S_1 \rangle + \frac{1}{2s} \|S_2 - S_1\|_q^2 \\ \implies J_\lambda(S_2) &\leq J_\lambda(S_1) + \langle \nabla_S J_\lambda(S_1), S_2 - S_1 \rangle + \frac{1}{2s} \|S_2 - S_1\|_2^2 \end{aligned}$$

A symmetric property holds for  $(s, l_2)$ -strong convexity of  $K_\lambda(\pi)$  which is implied by  $(s, l_p)$ -strong convexity,  $1 \leq p \leq 2$ . By Assumption 4.1,

$$J_\lambda(S_{\theta_2}) - J_\lambda(S_{\theta_1}) - \langle \nabla_S J_\lambda(S_{\theta_1}), S_{\theta_2} - S_{\theta_1} \rangle \leq \frac{1}{2s} \|S_{\theta_2} - S_{\theta_1}\|_2^2 \leq \frac{\rho_M}{2s} \|\theta_2 - \theta_1\|_2^2. \quad (4)$$

To establish smoothness, it remains to bound  $\langle \nabla_S J_\lambda(S_{\theta_1}), S_{\theta_2} - S_{\theta_1} \rangle$ . Set  $v = \nabla_S J_\lambda(S_{\theta_1}) \in \mathbb{R}^N$  and consider the first-order Taylor expansion in  $\theta$  of  $\langle v, S_\theta \rangle$  evaluated at  $\theta = \theta_2$ . Applying Lagrange's

form of the remainder, there exists  $0 < c < 1$  such that

$$\begin{aligned} \langle v, S_{\theta_2} \rangle &= \langle v, S_{\theta_1} \rangle + \langle v, J_{\theta}^S(S_{\theta_2} - S_{\theta_1}) \rangle \\ &\quad + \frac{1}{2} \sum_{i=1}^n v_i (\theta_2 - \theta_1)^T [D_{\theta}^2(S_{\theta_1}(x_i) + c(S_{\theta_2}(x_i) - S_{\theta_1}(x_i)))] (\theta_2 - \theta_1) \end{aligned}$$

and so by Cauchy-Schwartz,

$$\langle v, S_{\theta_2} - S_{\theta_1} \rangle \leq \langle v, J_{\theta}^S(S_{\theta_2} - S_{\theta_1}) \rangle + \frac{\|D_{\theta}^2\|}{2} \sqrt{N} \|v\|_2 \|\theta_2 - \theta_1\|_2 \leq \frac{\rho_M}{2s} \|\theta_2 - \theta_1\|_2^2.$$

The final inequality follows by taking  $C_h \geq \lambda \sqrt{N} \sup_v \|v\|_2$ . This supremum is bounded by assumption that  $\Theta \subseteq B(0, R)$ . Plugging in  $v = \nabla_S J_{\lambda}(S_{\theta_1})$ , we have

$$\begin{aligned} \langle \nabla_S J_{\lambda}(S_{\theta_1}), S_{\theta_2} - S_{\theta_1} \rangle &\leq \langle \nabla_S J_{\lambda}(S_{\theta_1}), J_{\theta}^S(S_{\theta_2} - S_{\theta_1}) \rangle + \frac{\rho_M}{2s} \|\theta_2 - \theta_1\|_2^2 \\ &= \langle \nabla_{\theta} J_{\lambda}(S_{\theta_1}), \theta_2 - \theta_1 \rangle + \frac{\rho_M}{2s} \|\theta_2 - \theta_1\|_2^2. \end{aligned}$$

Returning to (4), we have

$$J_{\lambda}(S_{\theta_2}) - J_{\lambda}(S_{\theta_1}) \leq \langle \nabla_{\theta} J_{\lambda}(S_{\theta_1}), \theta_2 - \theta_1 \rangle + \frac{\rho_M}{s} \|\theta_2 - \theta_1\|_2^2.$$

from which Lemma B.1 follows.  $\square$

**Lemma B.2** (Gradient Descent). *Gradient descent over the parameters  $\theta$  with learning rate  $\eta = \frac{s}{2\rho_M}$  converges in  $T$  iterations to parameters  $\theta_t$  satisfying  $J_{\lambda}(S_{\theta_t}) - J_{\lambda}(S^*) \leq \left(\frac{2\kappa R^2}{s}\right) \frac{1}{T}$  where  $\kappa = \frac{\rho_M}{\rho_m}$  is the condition number.*

*Proof.* Fix  $\theta_0$  and set  $\theta_{t+1} = \theta_t - \eta \nabla_{\theta} J_{\lambda}(S_{\theta_t})$ . The step size  $\eta$  is chosen so that by Lemma B.1,  $J_{\lambda}(S_t) - J_{\lambda}(S_{t+1}) \geq \frac{s}{2\rho_M} \|\nabla_{\theta} J_{\lambda}(S_{\theta_t})\|_2^2$ .

By convexity,  $J_{\lambda}(S^*) \geq J_{\lambda}(S_{\theta_t}) + \langle \nabla_S J_{\lambda}(S_{\theta_t}), S^* - S_{\theta_t} \rangle$ , so that

$$\|\nabla_{\theta} J_{\lambda}(S_{\theta_t})\|_2^2 \geq \rho_m \|\nabla_S J_{\lambda}(S_{\theta_t})\|_2^2 \geq (J_{\lambda}(S_{\theta_t}) - J_{\lambda}(S^*))^2 \left( \frac{\rho_m}{\|S_{\theta_t} - S^*\|_2^2} \right).$$

Setting  $\Delta_t = J_{\lambda}(S_{\theta_t}) - J_{\lambda}(S^*)$ , this implies  $\Delta_t \geq \Delta_{t+1} + \Delta_t^2 \left( \frac{s\rho_m}{2\rho_M \|S_{\theta_t} - S^*\|_2^2} \right)$  and thus  $\Delta_t \leq \left[ T \left( \frac{s\rho_m}{2\rho_M \|S_{\theta_t} - S^*\|_2^2} \right) \right]^{-1}$ . The claim follows from  $\|S_{\theta_t} - S^*\|_2 < R$ .  $\square$

Theorem 4.2 follows immediately from Lemmas B.1 and B.2.  $\square$

**Theorem 4.3** – Stability of Regularized OT Problem. *Suppose  $K_{\lambda}(\pi)$  is  $s$ -strongly convex in  $l_1$  norm and let  $\mathcal{L}(\varphi, \psi, \pi)$  be the Lagrangian of the regularized optimal transport problem. For  $\hat{\varphi}, \hat{\psi}$  which are  $\epsilon$ -approximate maximizers of  $J_{\lambda}(\varphi, \psi)$ , the pseudo-plan  $\hat{\pi} = M_f(V(x, y; \hat{\varphi}, \hat{\psi}))\sigma(x)\tau(y)$  satisfies*

$$|\hat{\pi} - \pi^*|_1 \leq \sqrt{\frac{2\epsilon}{s}} \leq \frac{1}{s} \left| \nabla_{\hat{\pi}} \mathcal{L}(\hat{\varphi}, \hat{\psi}, \hat{\pi}) \right|_1.$$

*Proof.* For indices  $i$ , denote by  $S_i$  the tuple  $(\varphi_i, \psi_i, \pi_i)$ . The regularized optimal transport problem has Lagrangian  $\mathcal{L}(\varphi, \psi, \pi)$  given by

$$\mathcal{L}(\varphi, \psi, \pi) = \mathbb{E}_{\pi}[c(x, y)] + \lambda H_f(\pi) + \mathbb{E}_{\sigma}[\varphi(x)] - \mathbb{E}_{\pi}[\varphi(x)] + \mathbb{E}_{\tau}[\varphi(y)] - \mathbb{E}_{\pi}[\psi(y)]$$

Because  $\mathcal{L}(\varphi, \psi, \pi)$  is a sum of  $K_{\lambda}(\pi)$  and linear terms, the Lagrangian inherits  $s$ -strong convexity w.r.t. the argument  $\pi$ :

$$\mathcal{L}(S_2) \geq \mathcal{L}(S_1) + \langle \nabla \mathcal{L}(S_1), S_2 - S_1 \rangle + \frac{s}{2} |\pi_2 - \pi_1|_1^2.$$

Letting  $S^* = (\varphi^*, \psi^*, \pi^*)$  be the optimal solution and  $\hat{S} = (\hat{\varphi}, \hat{\psi}, \hat{\pi})$  be an  $\epsilon$ -approximation, it follows that

$$\epsilon \geq \mathcal{L}(\hat{S}) - \mathcal{L}(S^*) \geq \frac{s}{2} |\hat{\pi} - \pi^*|_1^2 \implies |\hat{\pi} - \pi^*| \leq \sqrt{\frac{2\epsilon}{s}}. \quad (5)$$

Additionally, note that strong convexity implies a Polyak-Łojasiewicz (PL) inequality w.r.t.  $\hat{\pi}$ .

$$s \left( \mathcal{L}(\hat{S}) - \mathcal{L}(S^*) \right) \leq \frac{1}{2} |\nabla_{\pi} \mathcal{L}(\hat{S})|_1^2. \quad (6)$$

The second inequality follows from (5) and the PL inequality (6). □

## B.1 Statistical Estimation of Sinkhorn Plans

We consider estimating an entropy regularized OT plan when  $\mathcal{Y} = \mathcal{X}$ . Let  $\hat{\sigma}, \hat{\tau}$  be empirical distributions generated by drawing  $n \geq 1$  i.i.d. samples from  $\sigma, \tau$  respectively. Let  $\pi_n^\lambda$  be the Sinkhorn plan between  $\hat{\sigma}$  and  $\hat{\tau}$  at regularization  $\lambda$ , and let  $D := \text{diam}(\mathcal{X})$ . For simplicity, we also assume that  $\sigma$  and  $\tau$  are sub-Gaussian. We also assume that  $n$  is fixed. Under these assumptions, we will show that  $W_1(\pi_n^\lambda, \pi^\lambda) \lesssim n^{-1/2}$ .

The following result follows from Proposition E.4 and E.5 of of Luise et al. [18] and will be useful in deriving the statistical error between  $\pi_n^\lambda$  and  $\pi^\lambda$ . This result characterizes fast statistical convergence of the Sinkhorn potentials as long as the cost is sufficiently smooth.

**Proposition B.3.** *Suppose that  $c \in \mathcal{C}^{s+1}(\mathcal{X} \times \mathcal{X})$ . Then, for any  $\sigma, \tau$  probability measures supported on  $\mathcal{X}$ , with probability at least  $1 - \tau$ ,*

$$\|v - v_n\|_\infty, \|u - u_n\|_\infty \lesssim \frac{\lambda e^{3D/\lambda} \log 1/\tau}{\sqrt{n}},$$

where  $(u, v)$  are the Sinkhorn potentials for  $\sigma, \tau$  and  $(u_n, v_n)$  are the Sinkhorn potentials for  $\hat{\sigma}, \hat{\tau}$ .

Let  $\pi_n^\lambda = M_n \sigma_n \tau_n$  and  $\pi^\lambda = M \sigma \tau$ . We recall that

$$M(x, y) = \frac{1}{e} \exp \left( \frac{1}{\lambda} (\varphi(x) + \psi(y) - c(x, y)) \right),$$

$$M_n(x, y) = \frac{1}{e} \exp \left( \frac{1}{\lambda} (\varphi_n(x) + \psi_n(y) - c(x, y)) \right),$$

We note that  $M$  and  $M_n$  are uniformly bounded by  $e^{3D/\lambda}$  [18] and  $M$  inherits smoothness properties from  $\varphi, \psi$ , and  $c$ .

We can write (for some optimal, bounded, 1-Lipschitz  $f_n$ )

$$\begin{aligned} W_1(\pi_n^\lambda, \pi^\lambda) &= \left| \int f_n \pi_n^\lambda - \int f_n \pi^\lambda \right| \\ &\leq \left| \int f_n (H_n - H) \sigma_n \tau_n \right| + \left| \int f_n H (\sigma_n \tau_n - \sigma \tau) \right| \\ &\leq |f_n|_\infty |H_n - H|_\infty + \left| \int f_n H (\sigma_n \tau_n - \sigma \tau) \right|. \end{aligned} \quad (7)$$

If  $\sigma$  and  $\tau$  are  $\beta^2$  subGaussian, then we can bound the second term with high probability:

$$\mathbb{P} \left( \left| \frac{1}{n^2} \sum_i \sum_j f_n(X_i, Y_j) H(X_i, Y_j) - \mathbb{E}_{\sigma \times \tau} f_n(X, Y) H(X, Y) \right| > t \right) < e^{-n^2 \frac{t^2}{2\beta^2}}.$$

Setting  $t = \sqrt{2} \log(\delta) \beta / n$  in this expression, we get that w.p. at least  $1 - \delta$ ,

$$\left| \frac{1}{n^2} \sum_i \sum_j f_n(X_i, Y_j) H(X_i, Y_j) - \mathbb{E}_{\sigma \times \tau} f_n(X, Y) H(X, Y) \right| < \frac{\sqrt{2} \beta \log \delta}{n}.$$



Now to bound the first term in (7), we use the fact that  $f_n$  is 1-Lipschitz and bounded by  $D$ . For the optimal potentials  $\varphi$  and  $\psi$  in the original Sinkhorn problem for  $\sigma$  and  $\tau$ , we use the result of Proposition B.3 to yield

$$\begin{aligned} |H_n(x, y) - H(x, y)| &= \left| \frac{1}{e} \exp\left(\frac{1}{\lambda}(\varphi_n(x) + \psi_n(y) - c(x, y))\right) - \frac{1}{e} \exp\left(\frac{1}{\lambda}(\varphi(x) + \psi(y) - c(x, y))\right) \right| \\ &= \frac{1}{e} \left| \exp\left(\frac{1}{\lambda}(\varphi(x) + \psi(y) - c(x, y))\right) \left(1 - \exp\left(\frac{\varphi(x) - \varphi_n(x)}{\lambda}\right) \exp\left(\frac{\psi(y) - \psi_n(y)}{\lambda}\right)\right) \right| \\ &\lesssim e^{3D/\lambda} |1 - e^{\frac{2}{\lambda\sqrt{n}}}| \\ &\lesssim \frac{e^{3D/\lambda}}{\lambda\sqrt{n}}. \end{aligned}$$

Thus, putting this all together,

$$W_1(\pi_n^\lambda, \pi^\lambda) \lesssim \frac{D}{\sqrt{n}} + \frac{1}{n}.$$

Interestingly, the rate of estimation of the Sinkhorn plan breaks the curse of dimensionality. It must be noted, however, that the exponential dependence of Proposition B.3 on  $\lambda^{-1}$  implies we can only attain these fast rates in appropriately large regularization regimes.

## B.2 Log-concavity of Sinkhorn Factor

The optimal entropy regularized Sinkhorn plan is given by

$$\pi^*(x, y) = \frac{1}{e} \exp\left(\frac{1}{\lambda}(\varphi^*(x) + \psi^*(y) - c(x, y))\right) \sigma(x)\tau(y).$$

This implies that the conditional Sinkhorn density of  $Y|X$  is

$$\pi^*(y|x) = \frac{1}{e} \exp\left(\frac{1}{\lambda}(\varphi^*(x) + \psi^*(y) - c(x, y))\right) \tau(y).$$

The optimal potentials satisfy fixed point equations. In particular,

$$\psi^*(y) = -\lambda \log \int \exp\left[-\frac{1}{\lambda}(c(x, y) - \varphi^*(x))\right] d\sigma(x).$$

Using this result, one can prove the following lemma.

**Lemma B.4** ([1]). *For the cost  $\|x - y\|^2$ , the map*

$$h(y) = \exp\left(\frac{1}{\lambda}(\varphi^*(x) + \psi^*(y) - \|x - y\|^2)\right)$$

*is log-concave.*

*Proof.* The proof comes by differentiating the map. We calculate the gradient,

$$\nabla \log h(y) = -2 \frac{y - x}{\lambda} + \frac{2 \int \exp\left[-\frac{1}{\lambda}(\|x - y\|^2 - \varphi^*(x))\right] (y - x) d\sigma(x)}{\int \exp\left[-\frac{1}{\lambda}(\|x - y\|^2 - \varphi^*(x))\right] d\sigma(x)}$$

and the Hessian,

$$\begin{aligned}
\nabla^2 \log h(y) &= -2 \frac{I}{\lambda} \\
&+ \frac{4}{\lambda^2} \frac{\int \exp \left[ -\frac{1}{\lambda} (\|x - y\|^2 - \varphi^*(x)) \right] (y - x) d\sigma(x) \int \exp \left[ -\frac{1}{\lambda} (\|x - y\|^2 - \varphi^*(x)) \right] (y - x)^\top d\sigma(x)}{\left( \int \exp \left[ -\frac{1}{\lambda} (\|x - y\|^2 - \varphi^*(x)) \right] d\sigma(x) \right)^2} \\
&- \frac{4}{\lambda^2} \frac{\int \exp \left[ -\frac{1}{\lambda} (\|x - y\|^2 - \varphi^*(x)) \right] (y - x)(y - x)^\top d\sigma(x)}{\int \exp \left[ -\frac{1}{\lambda} (\|x - y\|^2 - \varphi^*(x)) \right] d\sigma(x)} \\
&+ 2I/\lambda \frac{\int \exp \left[ -\frac{1}{\lambda} (\|x - y\|^2 - \varphi^*(x)) \right] d\sigma(x)}{\int \exp \left[ -\frac{1}{\lambda} (\|x - y\|^2 - \varphi^*(x)) \right] d\sigma(x)} \\
&= -\frac{4}{\lambda^2} \left( -\frac{\int \exp \left[ -\frac{1}{\lambda} (\|x - y\|^2 - \varphi^*(x)) \right] (y - x) d\sigma(x) \int \exp \left[ -\frac{1}{\lambda} (\|x - y\|^2 - \varphi^*(x)) \right] (y - x)^\top d\sigma(x)}{\left( \int \exp \left[ -\frac{1}{\lambda} (\|x - y\|^2 - \varphi^*(x)) \right] d\sigma(x) \right)^2} \right. \\
&\left. + \frac{\int \exp \left[ -\frac{1}{\lambda} (\|x - y\|^2 - \varphi^*(x)) \right] (y - x)(y - x)^\top d\sigma(x)}{\int \exp \left[ -\frac{1}{\lambda} (\|x - y\|^2 - \varphi^*(x)) \right] d\sigma(x)} \right)
\end{aligned}$$

In the last term, we recognize that

$$\rho(x) = \frac{\exp \left[ -\frac{1}{\lambda} (\|x - y\|^2 - \varphi^*(x)) \right]}{\int \exp \left[ -\frac{1}{\lambda} (\|x - y\|^2 - \varphi^*(x)) \right] d\sigma(x)}$$

forms a valid density with respect to  $\sigma$ , and thus

$$\nabla^2 \log h(y) = -\frac{4}{\lambda^2} \text{Cov}_{\rho d\sigma}(X - y)$$

where we take the covariance matrix of  $X - y$  with respect to the density  $\rho d\sigma$ .  $\square$

Suppose, for sake of argument, that  $\tau(y)$  is  $\alpha$  strongly log-concave, and the function  $h(y)$  is  $\beta$  strongly log-concave. Then,  $\pi_{Y|X=x} \propto h(y)\tau(y)$ ,  $\alpha + \beta$  strongly log-concave. In particular, standard results on the mixing time of the Langevin diffusion implies that the diffusion for  $\pi_{Y|X=x}$  mixes faster than the diffusion for the marginal  $\tau$  alone. Also, as  $\lambda \rightarrow 0$ , the function  $h(y)$  concentrates around  $\varphi_{OT}(x) + \psi_{OT}(y) - \|x - y\|^2$ , where  $\varphi_{OT}$  and  $\psi_{OT}$  are the optimal transport potentials. In particular, if there exists an optimal transport map between  $\sigma$  and  $\tau$ , then  $h(y)$  concentrates around the unregularized optimal transport image  $y = T(x)$ .

## C Experimental Details

### C.1 Network Architectures

Our method integrates separate neural networks playing the roles of *unconditional score estimator*, *compatibility function*, and *barycentric projector*. In our experiments each of these networks uses one of two main architectures: a fully connected network with ReLU activations, and an image-to-image architecture introduced by Song and Ermon [24] that is inspired by architectures for image segmentation.

For the first network type, we write ‘‘ReLU FCN, Sigmoid output,  $w_0 \rightarrow w_1 \rightarrow \dots \rightarrow w_k \rightarrow w_{k+1}$ ,’’ for integers  $w_i \geq 1$ , to indicate a  $k$ -hidden-layer fully connected network whose internal layers use ReLU activations and whose output layer uses sigmoid activation. The hidden layers have dimension  $w_1, w_2, \dots, w_k$  and the network has input and output with dimension  $w_0, w_{k+1}$  respectively.

For the second network type, we replicate the architectures listed in Song and Ermon [24, Appendix B.1, Tables 2 and 3] and refer to them by name, for example ‘‘NCSN 32<sup>2</sup> px’’ or ‘‘NCSNv2 32<sup>2</sup> px.’’

Our implementation of these experiments may be found in the supplementary code submission.

### C.2 Image Sampling Parameter Sheets

**MNIST  $\leftrightarrow$  USPS:** details for qualitative transportation experiments between MNIST and USPS in Figure 3 are given in Table 4.

**CelebA, Blur-CelebA  $\rightarrow$  CelebA:** we sample  $64^2$  px CelebA images. The Blur-CelebA dataset is composed of CelebA images which are first resized to  $32^2$  px and then resized back to  $64^2$  px, creating a blurred effect. The FID computations in Table 1 used a shared set of training parameters given in Table 5. The sampling parameters for each FID computation are given in Table 6.

**Synthetic Data:** details for the synthetic data experiment shown in Figure 2 are given in Table 7.

Problem Aspect	Hyperparameters	Numbers and details
Source	Dataset	USPS [19]
	Preprocessing	None
Target	Dataset	MNIST [13]
	Preprocessing	Nearest neighbor resize to $16^2$ px.
Score Estimator	Architecture	NCSN $32^2$ px, applied as-is to $16^2$ px images.
	Loss	Denoising Score Matching
	Optimization	Adam, lr = $10^{-4}$ , $\beta_1 = 0.9$ , $\beta_2 = 0.999$ . No EMA of model parameters.
	Training	40000 training iterations, 128 samples per minibatch.
Compatibility	Architecture	ReLU network with ReLU output activation, $256 \rightarrow 1024 \rightarrow 1024 \rightarrow 1$
	Regularization	$\chi^2$ Regularization, $\lambda = 0.001$ .
	Optimization	Adam, lr = $10^{-6}$ , $\beta_1 = 0.9$ , $\beta_2 = 0.999$
	Training	5000 training iterations, 1000 samples per minibatch.
Barycentric Projection	Architecture	ReLU network with sigmoid output activation, $256 \rightarrow 1024 \rightarrow 1024 \rightarrow 256$ . Input pixels are scaled to $[-1, 1]$ by $x \mapsto 2x - 1$ .
	Optimization	Adam, lr = $10^{-6}$ , $\beta_1 = 0.9$ , $\beta_2 = 0.999$
	Training	5000 training iterations, 1000 samples per minibatch.
Sampling	Annealing Schedule	7 noise levels decaying geometrically, $\tau_0 = 0.2154, \dots, \tau_6 = 0.01$ .
	Step size	$\epsilon = 5 \cdot 10^{-6}$
	Steps per noise level	$T = 20$
	Denoising? [9]	Yes
	$\chi^2$ SoftPlus threshold	$\alpha = 1000$

Table 4: Data and model details for the **USPS  $\rightarrow$  MNIST** qualitative experiment shown in Figure 3. For **MNIST  $\rightarrow$  USPS**, we use the same configuration with source and target datasets swapped.

Problem Aspect	Hyperparameters	Numbers and details
Source	Dataset	CelebA or Blur-CelebA [17]
	Preprocessing	140 <sup>2</sup> px center crop. If Blur-CelebA: nearest neighbor resize to 32 <sup>2</sup> px. Nearest neighbor resize to 64 <sup>2</sup> px. Horizontal flip with probability 0.5.
Target	Dataset	CelebA [17]
	Preprocessing	140 <sup>2</sup> px center crop. Nearest neighbor resize to 64 <sup>2</sup> px. Horizontal flip with probability 0.5.
Score Estimator	Architecture	NCSNv2 64 <sup>2</sup> px.
	Loss	Denoising Score Matching
	Optimization	Adam, lr = 10 <sup>-4</sup> , $\beta_1 = 0.9$ , $\beta_2 = 0.999$ . Parameter EMA at rate 0.999.
	Training	210000 training iterations, 128 samples per minibatch.
Compatibility	Architecture	ReLU network with ReLU output activation, 3 · 64 <sup>2</sup> → 2048 → ... → 2048 → 1 (8 hidden layers).
	Regularization	Varies in $\chi^2$ reg., $\lambda \in \{0.1, 0.1, 0.001\}$ , and KL reg., $\lambda \in \{0.1, 0.01, 0.005\}$ .
	Optimization	Adam, lr = 10 <sup>-6</sup> , $\beta_1 = 0.9$ , $\beta_2 = 0.999$
	Training	5000 training iterations, 1000 samples per minibatch.
Barycentric Projection	Architecture	NCSNv2 64 <sup>2</sup> px applied as-is for image generation.
	Optimization	Adam, lr = 10 <sup>-7</sup> , $\beta_1 = 0.9$ , $\beta_2 = 0.999$
	Training	20000 training iterations, 64 samples per minibatch.

Table 5: Training details for the **CelebA, Blur-CelebA** → **CelebA** FID experiment (Figure 2).

Problem	Noise ( $\tau_1, \tau_k$ )	Step Size	Steps	Denoising? [9]	$\chi^2$ SoftPlus Param.
$\chi^2, \lambda = 0.1$	(9, 0.01)	$15 \cdot 10^{-7}$	$k = 500$	Yes	$\alpha = 10$
$\chi^2, \lambda = 0.01$	—  —				
$\chi^2, \lambda = 0.001$	—  —				
KL, $\lambda = 0.1$	(90, 0.1)	$15 \cdot 10^{-7}$	$k = 500$	Yes	—
KL, $\lambda = 0.01$	—  —				
KL, $\lambda = 0.005$	(90, 0.1)	$1 \cdot 10^{-7}$	$k = 500$	Yes	—

Table 6: Sampling details for the **CelebA, Blur-CelebA** → **CelebA** FID experiment (Figure 2).

Problem Aspect	Hyperparameters	Numbers and details
Source	Dataset	Gaussian in $\mathbb{R}^{784}$ , Mean and covariance are that of MNIST
	Preprocessing	None
Target	Dataset	Unit gaussian in $\mathbb{R}^{784}$ .
	Preprocessing	None
Score Estimator	Architecture	None (score is given by closed form)
Compatibility	Architecture	ReLU network with ReLU output activation, 784 $\rightarrow$ 2048 $\rightarrow$ 2048 $\rightarrow$ 2048 $\rightarrow$ 2048 $\rightarrow$ 1
	Regularization	KL Regularization, $\lambda \in \{1, 0.5, 0.25\}$ .
	Optimization	Adam, lr = $10^{-6}$ , $\beta_1 = 0.9$ , $\beta_2 = 0.999$
	Training	5000 training iterations, 1000 samples per minibatch.
Sampling	Annealing Schedule	No annealing.
	Step size	$\epsilon = 5 \cdot 10^{-3}$
	Mixing steps	$T = 1000$
	Denoising? [9]	Not applicable.

Table 7: Sampling and model details for the synthetic experiment shown in Figure 2.